IOP Publishing Nano Express 2 (2021) 020014 https://doi.org/10.1088/2632-959X/abfd8c

NANO EXPRESS

PAPER

Single step synthesis of WO_3 nanoparticles by wire explosion process and its photocatalytic behaviour

Prem Ranjan[1], **H. Suematsu**[2] and **R. Sarathi**[3]

[1] Department of Electrical and Electronic Engineering, The University of Manchester, Manchester, M13 9PL, United Kingdom
[2] Extreme Energy-Density Research Institute, Nagaoka University of Technology, Nagaoka 940-2188, Japan
[3] Department of Electrical Engineering, Indian Institute of Technology Madras, Chennai, 600 036 India

E-mail: prem.ranjan@manchester.ac.uk

Keywords: Nanoparticles, wire explosion, tungsten oxide, methylene blue, photodegradation

RECEIVED
21 December 2020

REVISED
7 April 2021

ACCEPTED FOR PUBLICATION
30 April 2021

PUBLISHED
11 May 2021

Tungsten (W) wires are exploded in oxygen ambience to get tungsten oxide (WO_3) nanoparticles (NPs). Energy stored in the capacitors (E_C) is used to overcome the sublimation energy of wire. Energy ratio (K, ratio of E_C and sublimation energy) and oxygen pressure (P) are two control parameters for the particle phase and morphology in the wire explosion process. X-ray diffraction (XRD) patterns confirmed the partial oxidation of W for low values of K. For $K = 2$, oxidation increases with increase in P. For $K = 10$, complete oxidation was achieved irrespective of P. Particles are spherical in shape as observed from scanning electron microscope (SEM) and transmission electron microscope (TEM) micrographs. Particle size follows a log-normal distribution with a least mean size of 24.1 nm. UV-vis diffuse reflectance spectroscopy (DRS) was used to measure the absorbance of NPs (complete WO_3 with least mean size) for band gap measurement. The band gap was found to be 2.92 eV (visible region). NPs are used as photocatalyst to degrade aqueous solution of methylene blue (MB) under visible light irradiation. 500 mg l^{-1} of WO_3 NPs were optimum to degrade 10 mg l^{-1} MB in 120 min.

1. Introduction

Functional materials and its nanostructures attract researchers due to its unique characteristics. Nano dimensions provide a wide control over the properties of a material. Nanoparticles (NPs; size range from 1 to 100 nm) are extensively studied for their unique traits for a particular application. Metal oxide NPs are an important constituent of many ceramic structures and smart devices. Nanostructure of tungsten oxide (WO_3), a transition metal oxide has versatile characteristics, a reason for being investigated in the fields of condensed matter physics to solid-state chemistry [1]. It finds its application in numerous fields like development of gas sensors [2], electrochromic devices [3], dye-sensitized solar cells [4], for field-emission applications [5], high-temperature superconductors [6] and as photocatalysts [7].

As a phtocatalyst, WO_3 is widely applied in the areas of air purification [8], CO_2 photoreduction [9], treatment of heavy metals [10], hydrogen evolution from splitting water [11], photodegradation of water pollutant [12], etc. Degradation of water pollutant like dye needs a lot of attention as the wastewater discharge from textile industries pollutes the surface water and in long run ground water too. Dye degradation using photocatalysis is widely researched using a number of metal oxide nanoparticles [13]. Starting from titanium dioxide (TiO_2), a classical photocatalyst for dye degradation [14] to zinc oxide (ZnO) NPs need ultra-violet (UV) light irradiation to overcome its band gap barrier [15]. But, sunlight consists of only 7% of the UV light. Visible light constituents for 40% of the sunlight we get on earth [16]. So, it is necessary to utilize NPs which can be used in the visible light.

WO_3 provides a viable solution as its band gap lies in the visible region [1]. Many researchers showed the applicability of WO_3 NPs for photodegaration of water pollutant. A number of methods were employed for synthesis of WO_3 NPs for this purpose, e.g. hydrothermal method [17], precipitation method [18], reverse microemulsion process [19], by annealing hexagonal ammonium tungsten bronze [20], flame aerosol route [21],

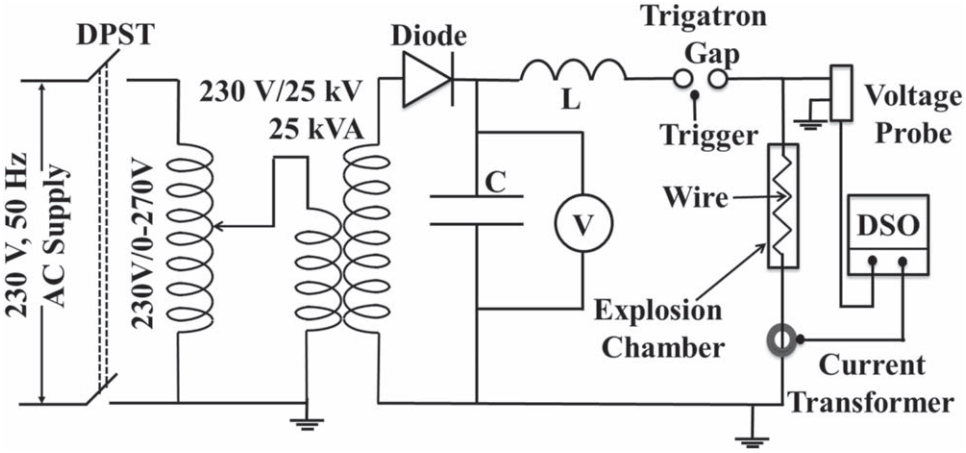

Figure 1. Schematic of wire explosion setup used.

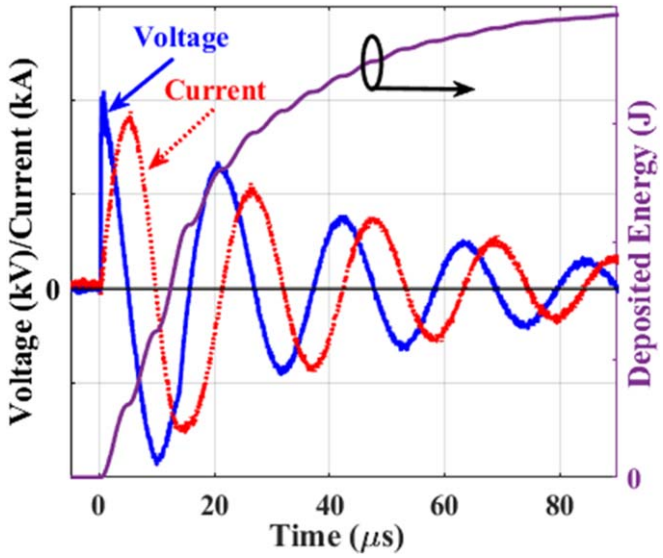

Figure 2. Voltage, current and energy deposited to the wire during wire explosion process.

ultrasound synthesis method assisted with CTAB [22], sol-gel method [23], spray-pyrolysis method with colloidal templating [24], arc discharge [25] etc. These synthesizing methods require many steps and/or various precursors. Wire explosion process (WEP) provides a single step method to produce NPs with least number of precursors.

WEP is also termed as pulsed wire discharge (PWD) or electric wire discharge (EWD), which needs wire and the reacting/cooling fluid as the starting materials [26–31]. In present work, tungsten (W) wires were used in oxygen ambience. High current was passed through the wire causing joule heating which leads to vaporisation of the wire. W vapour/plasma reacts with oxygen gas to form WO_3 NPs after simultaneous fast quenching. NPs synthesized by WEP were applied in a number of fields including photocatalysis under UV-light irradiation using WEP synthesized ZnO [30] and TiO_2 [31]. There is scarce report on usability of WEP synthesized NPs in visible light range. Previously, Arvinth *et al* attempted to synthesize WO_3 NPs by WEP but could not get complete oxidation of W vapour as there were traces of W were found in XRD patterns of their work [32].

Hence, in the present work, pure WO_3 NPs are synthesized without any traces of W. Size and oxidation control are discussed with variation in energy and oxygen pressure. Band gap of produced NPs is measured for its usability in visible light. Photoactivity of WEP synthesized NPs has been investigated under visible light irradiation taking methylene blue (MB) as a representative pollutant in water. Kinetics and mechanism of photodegradation of MB will be discussed.

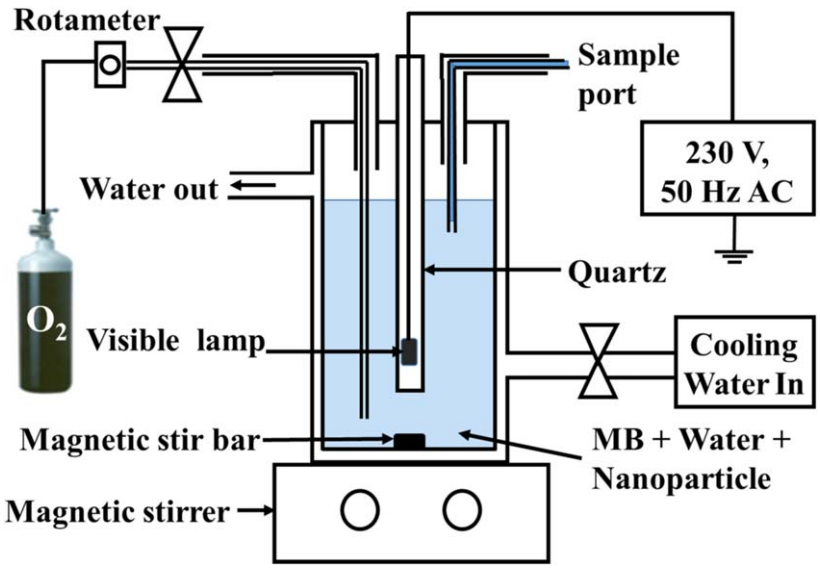

Figure 3. Schematic of photoactivity test setup.

Table 1. Experimental parameters for nanoparticle synthesis.

Wire material	Tungsten, W
Diameter (mm)	0.3, 0.1
Length (mm)	30, 50, 135
Capacitor (μF)	3
Charging Voltage (kV)	19,21,24,27
Ambient oxygen pressure (kPa)	20,180

2. Experimental studies

2.1. Synthesis of WO_3 NPs by wire explosion process

Experimental setup used for the synthesis of NPs in this work is shown in figure 1. Wire of required dimension was fixed between the electrodes. The chamber was closed and vacuumed. Then, oxygen was purged in the exploding chamber till the required pressure (monitored by pressure gauge). Supply voltage of 230 V, 50 Hz AC was connected to a step-up transformer (230 V/25 kV, 25 kVA) through an autotransformer (230V/0-270V) to get the required voltage. The capacitor bank of total capacitance (C, 3 μF) was charged by the rectified voltage (V, diode was used for rectification). Energy ($E_C = 0.5CV^2$) stored in C was discharged to the wire after triggering a trigatron gap. The energy injection/deposition to the wire leads to heating of the wire with subsequent explosion. Energy left after wire heating was deposited in arc discharge leading to the expansion of vapour/plasma cloud. The vapour reacts and gets cool down simultaneously to yield NPs. Voltage and current during the explosion were measured using a voltage probe (Tektronix P6015A) and a current transformer (Pearson 101) respectively. Figure 2 shows the current, voltage and energy (integral sum of instantaneous power) deposited to the wire during explosion. Table 1 shows the experimental parameters used for the synthesis of NPs in present work. Based on the circuit parameters, it matches with the condition of an under damped RLC circuit [33] as per equation 1,

$$\frac{R}{2} < \sqrt{\frac{L}{C}} \tag{1}$$

The expression for the magnitude of current flow through the R, can be written as,

$$I(t) = \frac{Ve^{(-R/2L)t}}{\sqrt{(L/C) - (R^2/4)}} \sin\left(\sqrt{\frac{1}{LC} - \frac{R^2}{4L^2}}\, t\right). \tag{2}$$

The minimum energy per gram to vaporize the wire (sublimation energy), E_S can be written as,

$$E_S = C_S * (T_m - T_r) + C_f * (T_b - T_m) + h_m + h_v, \tag{3}$$

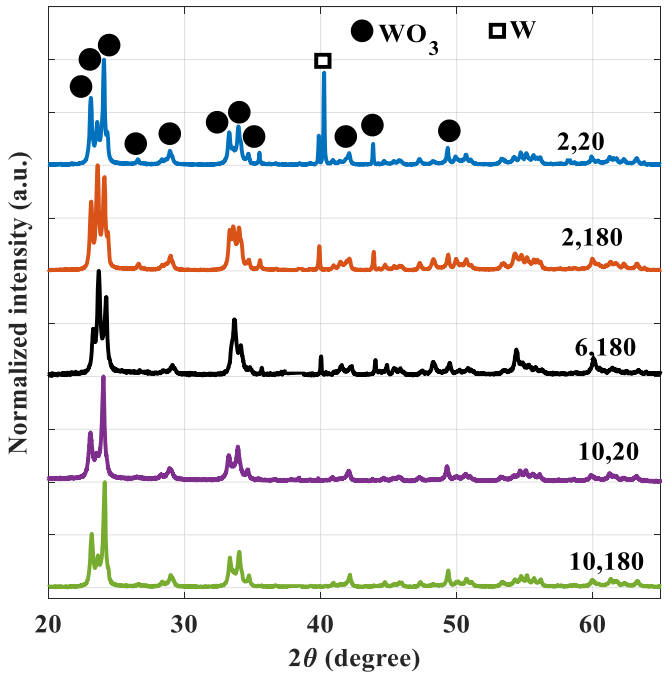

Figure 4. XRD patterns of nanoparticles produced by wire explosion process at different energy ratio, K and oxygen pressure, P (kPa).

where, C_S and C_f are specific heat in the solid and liquid state respectively, T_r, T_m and T_b are room, melting and boiling temperature of the metal respectively, and h_m and h_v are latent heat of fusion and vaporization of the material respectively. The data for the calculation were taken from CRC databook [34]. The energy ratio, K defined as the ratio of E_C and E_S is used in this work as the parameter to describe the effect of energy deposited to the wire. K and P are two parameters to control the morphology and/or phase of NPs produced by WEP.

2.2. Photoactivity test of NPs

Test pollutant, methylene blue (MB; Merck life sciences private limited, India) was dissolved in distilled water to make a stock solution of 1 g l^{-1}. For photodegradation, 10 mg l^{-1} MB solution was prepared from the stock solution. Figure 3 shows the photoreactor (30 cm height and volume of 130 ml, Heber scientific, India) used in this work. It is an immersion type reactor equipped with an outer cooling jacket (cools the reaction solution of MB and NPs by circulation of water with help of a pump), an oxygen port (flow was controlled by rotameter) and a port for taking out the sample. The cooling (water jacket) keeps the reaction solution at room temperature. A visible lamp (230 V, 150 W) was used for the irradiation of solution. Magnetic stirring keeps the nanoparticles in solution and prevents it from settling down.

2.3. Analytical methods

The phase of WEP-synthesized NPs was determined using an X-ray diffraction (XRD) technique. Data was obtained from Rigaku Smartlab X-Ray diffractometer with nickel-filtered Cu Kα radiation ($\lambda = 0.154$ nm) at 40 kV and 100 mA, and Rietveld refinement was carried out using X'pert High Score software. Morphology was observed using a scanning electron microscope (SEM, FEI Quanta FEG 200) and a transmission electron microscope (TEM, Tecnai T20). TEM samples were prepared by dropping two droplets of mixture of a pinch of NPs and acetone on carbon coated copper grid. Particle sizes were determined using ImageJ software. The band gap was measured using absorbance spectrum given by UV-vis diffused reflectance spectroscopy (DRS, JASCO V-650 spectrophotometer ISV-722) with $BaSO_4$ as reference.

10 mg l^{-1} MB solution in distilled water was used for photoactivity test. Synthesized NPs of different quantities were mixed in 100 ml of MB solution and stirred for 30 min to reach the adsorption-desorption equilibrium. 50 ml minute^{-1} of oxygen flow was maintained in the reactor solution with continuous stirring and visible light irradiation. 3 ml of solution was collected through port of setup for analysis at regular intervals. Absorbance of solutions were measured using UV-vis spectrophotometer (Shimadzu, Japan). Ratio of C and C_0 was defined as the degradation ratio, D as follows,

$$\text{Degradation ratio, } D = C/C_0 \tag{4}$$

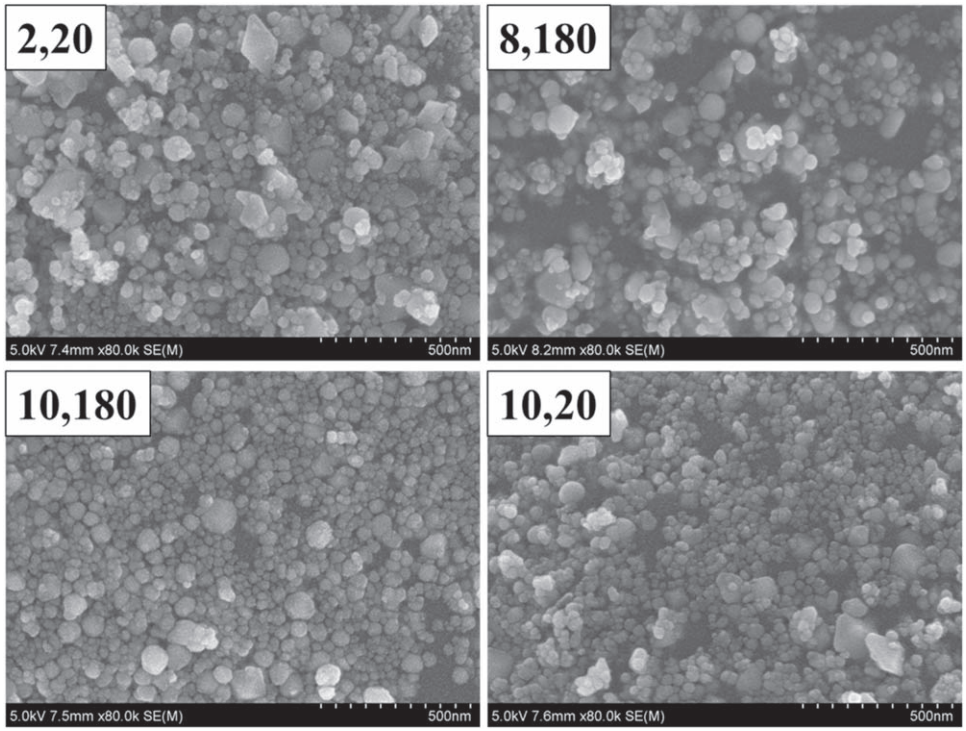

Figure 5. SEM images of nanoparticles produced by wire explosion process at different energy ratio, K and oxygen pressure, P (kPa).

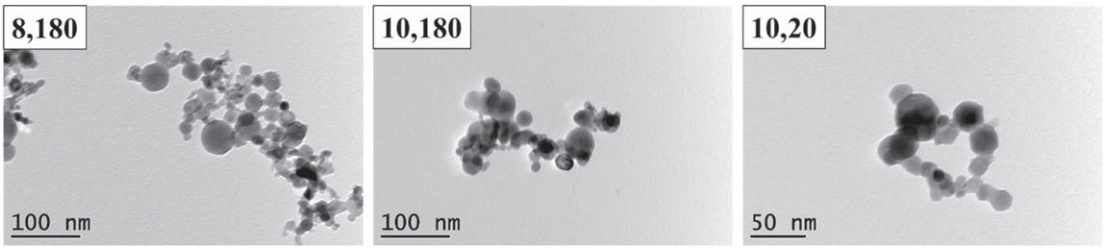

Figure 6. TEM images of nanoparticles produced by wire explosion process at different energy ratio, K and oxygen pressure, P (kPa).

Where, C_0 is the absorbance value of untreated methylene blue solution and C is the absorbance value of treated solution for different interval of time. Absorbance was measured at 663 nm.

3. Results and discussion

3.1. XRD studies

Figure 4 shows the XRD patterns of NPs produced by WEP after exploding tungsten (W) wire at different K and in different oxygen pressure, P. The patterns match with standard pattern of WO_3 (JCPDS card no.– 20-1324) and for K other than 10, extra peaks of W (JCPDS card no.–47-1319, 100% peak at 40°) was detected. For $K = 10$, complete oxidation of W vapour/plasma was achieved irrespective of the oxygen pressure used in the present work. For $K = 2$, the intensity of peak corresponding to W decreases with increase in P, attributed due to the more oxidation of metal vapour in presence of relatively more molecular oxygen. For $P = 180$ kPa, as we increase K from 2 to 6, decrease in intensity of peak corresponding to W indicates an increase in oxidation. This is due to decrease in density of metal vapour cloud produced after explosion for high energy deposition i.e. high K value [35]. For K =10, complete oxidation of W vapour was achieved irrespective of the value of P. The spread of vapour cloud was enough for the oxidation to WO_3. In short, it is possible to get complete oxidation of W vapour in WEP for higher energy deposition leading to WO_3 nanoparticle formation without any traces of W metal.

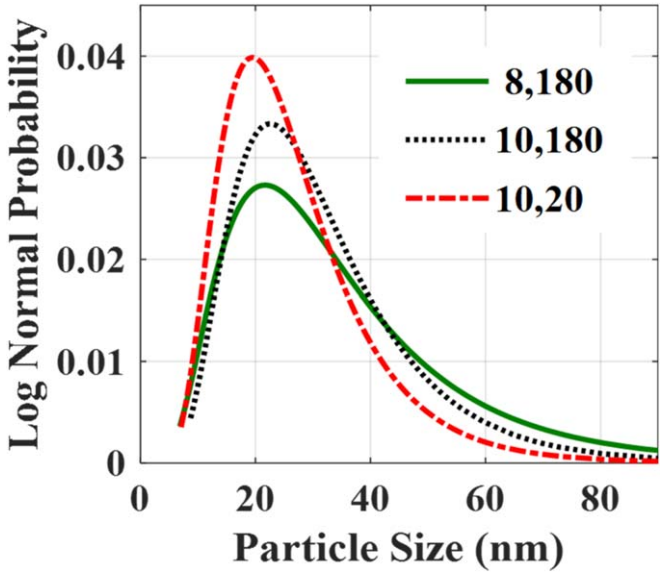

Figure 7. Particle size distribution of nanoparticles produced by wire explosion process at different energy ratio, K and oxygen pressure, P (kPa).

Table 2. Mean particle size and standard deviation of nanoparticles produced at different K and P values.

Sample (K,P in kPa)	Mean size(nm)	Standard deviation (nm)
8,180	30.1	1.7
10,180	28.2	1.6
10,20	24.1	1.6

3.2. SEM, TEM and particle size distribution studies

The morphology of NPs produced by WEP was checked through SEM and TEM micrographs. Figure 5 shows SEM images of NPs synthesized at different K and P values. Particles are spherical in shape except few. For low K value (K = 2), bigger size nanoparticles were there with some having submicron size. This is due to the formation of NPs from molten metal instead of from vapour at low energy deposition to the wire [27]. Figure 6 shows the TEM images of NPs. Particles size (Heywood diameter, diameter of circle with equivalent area to the area of 2-dimensional projection of 3-dimensional particles) varies from few to 100 nm for all the cases presented in figure 6. Particle size of about 500 NPs were measured and it fits into Log-normal distribution [36] as per equations 5–7,

$$f(d) = \frac{1}{\sqrt{2\pi}\, d \log \sigma_g} \exp\left(-\frac{(\log d - \log D_1)^2}{2(\log \sigma_g)^2}\right), \tag{5}$$

$$\sigma_g = \sqrt{\frac{\sum n_i (\log d - \log D_1)^2}{\sum n_i}}, \tag{6}$$

$$\log D_1 = \frac{\sum n_i \log d_i}{\sum n_i}. \tag{7}$$

where f(d) represents the log-normal distribution, d and D_1 are the particle and geometric mean diameter respectively, n_i and d_i are the number of particles and its diameter respectively, and σ_g is the geometrical standard deviation. Figure 7 shows the log-normal distribution of NPs synthesized by WEP. The corresponding mean size and standard deviation is shown in table 2. Mean size of NPs reduces with increase in K for P = 180 kPa. This is due to the fact that, more energy deposition leads to more expansion of metal vapour (keeping other parameters constant) due to increase in available energy in arc discharge after the explosion [27]. For K = 10, size of NPs decreases with decrease in P due to less dense vapour cloud formation after explosion for low value of K. In short, small size oxide NPs is formed for high energy deposition and/or lower P.

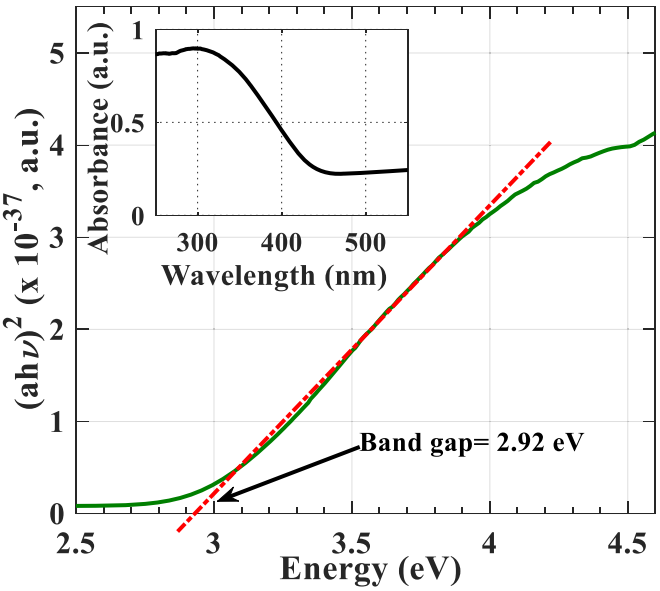

Figure 8. $(ah\nu)^2$ as a function of energy of nanoparticles produced by wire explosion process at energy ratio, K = 10 and oxygen pressure, P = 20 kPa (inset shows the absorbance for same).

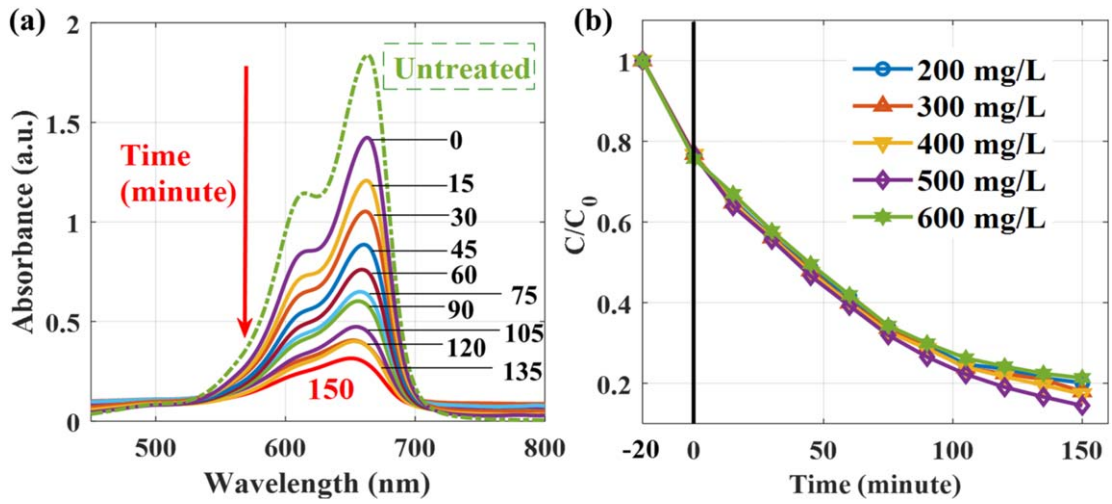

Figure 9. (a) Absorbance of untreated methylene blue solution (10 mg l^{-1}) and treated with NPs (500 mg l^{-1}) for different treatment times (in minutes) and (b) C/C_0 as a function of treatment time with varying NPs concentration.

3.3. Band gap measurement by UV-vis DRS study

Figure 8 (inset) shows the absorbance of WO_3 NPs produced by WEP at K = 10 and P = 20 kPa. The spectrum has a decrease in absorbance after 300 nm. Band gap of NPs was determined using equation 8 [37, 38] as follows,

$$\alpha h\nu = \mathrm{A}(h\nu - \mathrm{Eg})^{\mathrm{m}} \tag{8}$$

where, α is the absorption coefficient, h is Planck's constant, $h\nu$ is photon energy, and m = 0.5 for semiconductors with direct allowed transition. α is replaced by absorbance 'a' as it is directly proportional to 'a'. Energy of photons are defined by hc/λ; where c and λ are the speed of light and the wavelength respectively. Figure 8 shows the variation of $(ah\nu)^2$ as a function of energy (eV). Band gap of NPs is the value of energy on X-axis at which the extended linear portion of the curve crosses. The band gap of NPs produced at K = 10 and P = 20 kPa was found to be 2.92 eV which lies in visible region. It is comparable to the band gap of 2.88 eV for WO_3 NPs measured by Azbari *et al* [19]. In short, WO_3 NPs produced by WEP can be harnessed for photocatalysis in visible region.

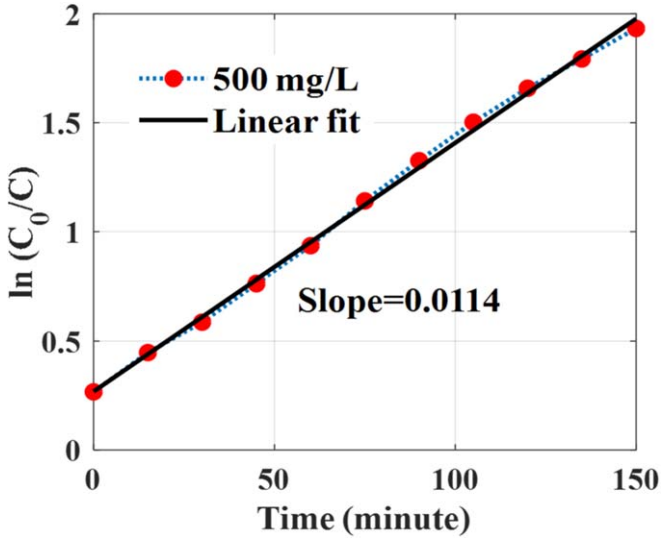

Figure 10. Kinetic curve of MB degradation with WO_3 NPs (500 mg l^{-1}).

3.4. Photocatalytic behaviour of WEP synthesized WO_3 nanoparticles

NPs produced at K = 10 and P = 20 kPa gives complete oxidised yield with least mean size of 24.1 nm (table 2) and a band gap of 2.92 eV (section 3.3). For photoactivity tests, NPs synthesized at these conditions were utilized in this work. Tests to demonstrate the effect of NPs size on the photoactivity was not carried out as the completely oxidised NPs has close size range (24–30 nm) as depicted from table 2. The influence of size on the photoactivity of NPs will be carried out in the next work. Figure 9(a) shows the absorbance of used aqueous solution of MB and treated solutions for different treatment time. The solution was treated with WO_3 NPs (500 mg l^{-1}) under visible light irradiation. Absorbance of MB decreases with increase in the treatment time indicating degradation and decolourisation of MB solution. Decolourisation was visible from the colour intensity of the solution. Figure 9(b) shows the variation of C/C_0 with treatment time for different concentration of WO_3 NPs in the solution mixture. It decreases with time for all the cases depicting the photocatalytic effect of WO_3 NPs.

As we increase the concentration of NPs from 200 mg l^{-1} in steps of 100 mg l^{-1} till 500 mg l^{-1}, C/C_0 has decreased with increasing concentration indicating more degradation. This is because of the availability of more number of reaction sites to generate electron-hole pairs with increase in number (concentration) of NPs [30, 31]. But, if the concentration of NPs was increased further to 600 mg l^{-1}, the C/C_0 value increases indicating a decrease in degradation. This is attributed to the fact that at higher concentration of NPs in solution, (i) NPs will tend to agglomerate leading to decrease in active sites, (ii) high turbidity of solution leads to inhibition and scattering of light which prevents all photon energy to reach NPs to produce electron-hole pairs for degradation reactions [15]. For 500 mg l^{-1} of WO_3, we achieved 86% degradation of MB solution (10 mg l^{-1}) for 150 min of treatment time. Martinez *et al* [18] observed about 90% degradation of rhodamine B dye (5 mg l^{-1}) in 150 min which is comparable as present work used 10 mg l^{-1} dye solution.

3.5. Kinetics and mechanism of photodegradation

Kinetics of photodegradation was studied using Langmuir–Hinshelwood model. As the concentration of MB is low (10 mg l^{-1}), we approximated the degradation kinetics using pseudo first order equation [37] given as

$$\ln\left(\frac{C_0}{C}\right) = k_{psuedo}t, \tag{9}$$

where k_{psuedo} is the pseudo-first-order rate constant (minute^{-1}) which is equal to the slope of the line indicating the variation of $\ln(C_0/C)$ as a function of time, t. Figure 10 shows the kinetics curve of MB degradation using WO_3 NPs as catalyst with a concentration of 500 mg l^{-1}. Linear fit for data has a slope of 0.0114 per minute.

The degradation of dye/pollutant in water comprises of many steps. The reactions involved in photodegradation is given as follows [18, 39]:

$$WO_3 + h\nu \rightarrow e^-_{cb} + h^+_{vb} \tag{10}$$

$$e^-_{cb} + O_2 \rightarrow \cdot O_2^- \tag{11}$$

$$h^+_{vb} + H_2O \rightarrow \cdot OH + H^+ \tag{12}$$

$$\bullet O_2^- + H^+ \rightarrow HO_2\bullet \quad (13)$$

$$2HO_2\bullet \rightarrow H_2O_2 + O_2 \quad (14)$$

$$H_2O_2 + \bullet O_2^- \rightarrow \bullet OH + OH^- + O_2 \quad (15)$$

$$h_{vb}^+ + OH^- \rightarrow \bullet OH \quad (16)$$

$$H_2O_2 + e_{cb}^- \rightarrow \bullet OH + OH^- \quad (17)$$

$$\text{Dye} + \bullet O_2^- + \bullet OH \rightarrow CO_2 + H_2O + \text{Degraded products} \quad (18)$$

where, equation 10 depicts the generation of holes (h_{vb}^+) and electrons (e_{cb}^-) from valance and conduction band of WO_3 NPs respectively. A semiconductor yields electron-hole pair if it is irradiated with photon energy more than its band gap energy. The reaction solution contains dissolved oxygen which reacts with electrons to give superoxide radical ($\bullet O_2^-$) as shown in equation 11. Water molecules react with holes to yield hydroxyl radical ($\bullet OH$) and hydrogen ion (equation 12). More hydroxyl ions are generated through reactions represented by equations 13–17 with formation of hydrogen peroxide (H_2O_2) and its radical. Superoxide and hydroxyl radicals are oxidising in nature which lead to degradation of pollutant to carbon dioxide (CO_2) and small degraded compounds as shown in equation 18.

4. Conclusions

Completely oxidized WO_3 NPs were successfully synthesized using wire explosion process. High energy and high pressure aids in oxidation of W vapour/plasma. Size of NPs decrease with increase in K and/or decrease in P. Particle size data follows log-normal distribution. Least mean size of NPs was found to be 24.1 nm. Band gap of NPs was found to be 2.92 eV by DRS measurement. Optimum quantity of NPs was found to be 500 mg/l for the degradation of 10 mg l^{-1} MB solution under visible light irradiation.

Data availability statement

The data that support the findings of this study are available upon reasonable request from the authors.

ORCID iDs

Prem Ranjan https://orcid.org/0000-0001-7840-9904

References

[1] Zheng H, Ou J Z, Strano M S, Kaner R B, Mitchell A and Kalantar-Zadeh K 2011 Nanostructured tungsten oxide - Properties, synthesis, and applications *Adv. Funct. Mater.* **21** 2175–96
[2] Siciliano T, Tepore A, Micocci G, Serra A, Manno D and Filippo E 2008 WO3 gas sensors prepared by thermal oxidization of tungsten *Sensors Actuators, B Chem.* **133** 321–6
[3] Ruan J, Thummavichai K, Lu Y, Zhu Y and Yan H 2018 Phase transition and optical absorption evolution of WO 3 nanoparticles induced by pressure *Mater. Res. Express* **5** 1–7
[4] Zheng H, Tachibana Y and Kalantar-Zadeh K 2010 Dye-sensitized solar cells based on WO3 *Langmuir* **26** 19148–52
[5] Fang X, Bando Y, Gautam U K, Ye C and Golberg D 2008 Inorganic semiconductor nanostructures and their field-emission applications *J. Mater. Chem.* **18** 509–22
[6] Deb S K 2008 Opportunities and challenges in science and technology of WO3 for electrochromic and related applications *Sol. Energy Mater. Sol. Cells* **92** 245–58
[7] Dong P, Hou G, Xi X, Shao R and Dong F 2017 WO3-based photocatalysts: morphology control, activity enhancement and multifunctional applications *Environ. Sci. Nano* **4** 539–57
[8] Balayeva N O, Fleisch M and Bahnemann D W 2018 Surface-grafted WO3/TiO2 photocatalysts: Enhanced visible-light activity towards indoor air purification *Catal. Today* **313** 63–71
[9] Wang W N, Soulis J, Jeffrey Yang Y and Biswas P 2014 'Comparison of CO2photoreduction systems: A review,' *Aerosol Air Qual. Res.* **14** 533–49
[10] Yang L *et al* 2010 Photocatalytic reduction of Cr(VI) on WO3 doped long TiO2 nanotube arrays in the presence of citric acid *Appl. Catal. B Environ.* **94** 142–9
[11] Nayak A K, Verma M, Sohn Y, Deshpande P A and Pradhan D 2017 Highly active tungsten oxide nanoplate electrocatalysts for the hydrogen evolution reaction in acidic and near neutral electrolytes *ACS Omega* **2** 7039–47
[12] Gondal M A, Sayeed M N and Alarfaj A 2007 Activity comparison of Fe2O3, NiO, WO3, TiO2 semiconductor catalysts in phenol degradation by laser enhanced photo-catalytic process *Chem. Phys. Lett.* **445** 325–30
[13] Ibhadon A and Fitzpatrick P 2013 Heterogeneous photocatalysis: recent advances and applications *Catalysts* **3** 189–218
[14] Nakata K and Fujishima A 2012 TiO2 photocatalysis: Design and applications *J. Photochem. Photobiol. C Photochem. Rev.* **13** 169–89
[15] Lee K M, Lai C W, Ngai K S and Juan J C 2016 Recent developments of zinc oxide based photocatalyst in water treatment technology: A review *Water Res.* **88** 428–48
[16] Kochevar I E, Pathak M A and PJ A 1999 Photophysics, photochemistry, and phobiology ed Fitzpatrick *Dermatology in General Medicine* (New York: McGraw-Hill)

[17] Huang J, Xiao L and Yang X 2013 WO3 nanoplates, hierarchical flower-like assemblies and their photocatalytic properties *Mater. Res. Bull.* **48** 2782–5
[18] Martínez D S, Martínez-De La Cruz A. and Cuéllar E L 2011 Photocatalytic properties of WO3 nanoparticles obtained by precipitation in presence of urea as complexing agent *Appl. Catal. A Gen.* **398** 179–86
[19] Abazari R, Mahjoub A R, Saghatforoush L A and Sanati S 2014 Characterization and optical properties of spherical WO3 nanoparticles synthesized via the reverse microemulsion process and their photocatalytic behavior *Mater. Lett.* **133** 208–11
[20] Szilágyi I M *et al* 2012 WO3 photocatalysts: Influence of structure and composition *J. Catal.* **294** 119–27
[21] Wang S, Lan Z and Huang Y 2016 Flame aerosol synthesis of tungsten trioxide powder: Particle morphology control and photodegradation activity under visible light irradiation *Powder Technol.* **294** 259–65
[22] Sánchez-Martíneza D, Gómez-Solísa C and Torres-Martíneza L M 2015 CTAB-assisted ultrasonic synthesis, characterization and photocatalytic properties of WO3 *Mater. Res. Bull.* **61** 165–72
[23] Ahmed B, Kumar S, Ojha A K, Donfack P and Materny A 2017 Facile and controlled synthesis of aligned WO 3 nanorods and nanosheets as an efficient photocatalyst material *Spectrochim. Acta - Part A Mol. Biomol. Spectrosc.* **175** 250–61
[24] Nandiyanto A B D, Arutanti O, Ogi T, Iskandar F, Kim T O and Okuyama K 2013 Synthesis of spherical macroporous WO3 particles and their high photocatalytic performance *Chem. Eng. Sci.* **101** 523–32
[25] Ashkarran A A, Zad A I, Ahadian M M and Ardakani S A M 2008 Synthesis and photocatalytic activity of WO3 nanoparticles prepared by the arc discharge method in deionized water *Nanotechnology* **19** 195709
[26] Kotov Y 2003 Electric explosion of wires as a method for preparation of nanopowders *J. Nanoparticle Res.* **5** 539–50
[27] Ranjan P, Nguyen D H, Tanaka K, Suematsu H, Jayaganthan R and Sarathi R 2019 Synthesis, characterisation and formation mechanism of Sn-0.75 Cu solder nanoparticles by pulsed wire discharge *Appl. Nanosci.* **9** 341–52
[28] Jiang W and Yatsui K 1998 Pulsed wire discharge for nanosize powder synthesis *IEEE Trans. Plasma Sci.* **26** 1498–501
[29] Suematsu H *et al* 2007 Pulsed wire discharge apparatus for mass production of copper nanopowders *Rev. Sci. Instrum.* **78** 2005–8
[30] Ranjan P, Singh R K, Suematsu H, Phillip L and Sarathi R 2017 'Synthesis of Nano-ZnO by wire explosion process and its photocatalytic activity *J. Environ. Chem. Eng.* **5** 1676–84
[31] Ranjan P, Nakagawa S, Suematsu H and Sarathi R 2018 Synthesis and photocatalytic activity of anatase/rutile TiO2 nanoparticles by wire explosion process *Ina. Lett.* **3** 189–96
[32] Aravinth S, Sankar B, Chakravarthi S R and Sarathi R 2011 Generation and characterization of nano tungsten oxide particles by wire explosion process *Mater. Charact.* **62** 248–55
[33] Hayt W H, Kemmerly J E and Durbin S M 2002 *Engineering Circuit Analysis* (New Delhi: Tata McGraw-Hill)
[34] Haynes W M 2014 *CRC Handbook of Chemistry and Physics* (Boca Raton: CRC Press)
[35] Ranjan P, Nguyen D H, Chen L, Cotton I, Suematsu H, Chakravarthy S R, Jayaganthan R and Sarathi R 2020 Kinetics of nanoparticle formation by wire explosion process *Nano Express.* **1** 010049 (1-11)
[36] Bernhardt C 1994 *Particle Size Analysis: Classification And Sedimentation Methods* (London: Chapman & Hall)
[37] Fox M A and Dulay M T 1993 Heterogeneous photocatalysis *Chem. Rev.* **93** 341–57
[38] López R and Gómez R 2012 Band-gap energy estimation from diffuse reflectance measurements on sol–gel and commercial TiO2: a comparative study *J. Sol Gel Sci. Technol.* **61** 1–7
[39] Hoffmann M R, Martin S T, Choi W and Bahnemann D W 1995 Environmental applications of semiconductor photocatalysis *Chem. Rev.* **95** 69–96